This copy is for personal use only. To order printed copies, contact *reprints@rsna.org*

Acute and Stress-related Injuries of Bone and Cartilage: Pertinent Anatomy, Basic Biomechanics, and Imaging Perspective[1]

Mini N. Pathria, MD, FRCP(C)
Christine B. Chung, MD
Donald L. Resnick, MD

Bone or cartilage, or both, are frequently injured related to either a single episode of trauma or repetitive overuse. The resulting structural damage is varied, governed by the complex macroscopic and microscopic composition of these tissues. Furthermore, the biomechanical properties of both cartilage and bone are not uniform, influenced by the precise age and activity level of the person and the specific anatomic location within the skeleton. Of the various histologic components that are found in cartilage and bone, the collagen fibers and bundles are most influential in transmitting the forces that are applied to them, explaining in large part the location and direction of the resulting internal stresses that develop within these tissues. Therefore, thorough knowledge of the anatomy, physiology, and biomechanics of normal bone and cartilage serves as a prerequisite to a full understanding of both the manner in which these tissues adapt to physiologic stresses and the patterns of tissue failure that develop under abnormal conditions. Such knowledge forms the basis for more accurate assessment of the diverse imaging features that are encountered following acute traumatic and stress-related injuries to the skeleton.

©RSNA, 2016

Online SA-CME
See www.rsna.org/education/search/ry

Learning Objectives:

After reading the article and taking the test, the reader will be able to:

- Describe the cycle of microdamage and remodeling in bone in response to daily activity
- Describe the normal morphology of articular cartilage and how it fails when injured
- Describe the anatomy and biomechanical properties of cortical bone and cancellous bone
- Discuss the sequence of changes that take place in bone during repetitive injury

Accreditation and Designation Statement

The RSNA is accredited by the Accreditation Council for Continuing Medical Education (ACCME) to provide continuing medical education for physicians. The RSNA designates this journal-based SA-CME activity for a maximum of 1.0 *AMA PRA Category 1 Credit™*. Physicians should claim only the credit commensurate with the extent of their participation in the activity.

Disclosure Statement

The ACCME requires that the RSNA, as an accredited provider of CME, obtain signed disclosure statements from the authors, editors, and reviewers for this activity. For this journal-based CME activity, author disclosures are listed at the end of this article.

[1] From the Department of Radiology (M.N.P.) and Radiology Service, VA San Diego Healthcare System (C.B.C.), UC San Diego Medical Center, 200 W Arbor Dr, San Diego, CA 92103; and Department of Radiology, UCSD Teleradiology and Education Center, La Jolla, Calif (D.L.R.). Received October 10, 2014; revision requested December 1; final revision received April 27, 2015; accepted May 11; final version accepted June 4; Final review January 20, 2016. **Address correspondence to** M.N.P. (e-mail: mpathria@ucsd.edu).

C.B.C. supported by the National Institutes of Health (grants R01DE022068 and R01AR064321) and by the U.S. Department of Veterans Affairs, Clinical Science Research and Development (Merit Award I01CX000625).

© RSNA, 2016

Failure of bone and cartilage may occur on a microscopic level alone or on both microscopic and macroscopic levels. Such failure relates to a mismatch between forces placed on the tissue and its ability to resist such forces, its strength. Skeletal strength is dependent on the material properties of its composite tissues. Therefore, to understand the manner in which bone and cartilage fail following an acute episode of trauma or repetitive stress, an initial short review of the embryology and macroscopic and microscopic anatomy is required. Following this, basic biomechanical principles are addressed that explain the patterns of failure occurring in the cartilage, subchondral bone plate, and cortical and cancellous bone that are encountered clinically.

Skeletal Development and Growth

Bone develops according to two distinct processes: intramembranous ossification and endochondral ossification (1,2). Intramembranous ossification involves bone formation arising directly in highly vascular sheets of condensed primitive mesenchyme. Endochondral bone formation, which is the more dominant process, relates to orderly and progressive ossification of a template composed of cartilage, forming primary and secondary ossification centers that eventually merge to form a single structure.

Intramembranous ossification is initiated by the proliferation of sheets of mesenchymal cells, followed by their transformation into osteoprogenitor cells and later osteoblasts that secrete a meshwork composed of collagen fibers and amorphous ground substance (1). This primitive osteoid, over time, is characterized by increasing regions and layers of calcified and ossified tissue that, in certain regions, maintain vascular spaces that become sites of hematopoietic tissue. Sites of intramembranous bone formation include the bones of the cranial vault, although a similar process occurs on the surface of most bones where the covering periosteum represents the mesenchymal tissue responsible for the development of a shell of compact cortical bone. The outer and inner surfaces of the cortex are covered by fibrous and collagenous layers of tissue, designated the periosteum and endosteum, respectively. Both layers contain all of the cells essential to bone turnover. The periosteal layer is thicker, less cellular, and firmly anchored to the bone by penetrating collagen fibers. The periosteum is more adherent to the cortex in the mature skeleton, compared with the immature skeleton, explaining the ease by which the periosteum is lifted by hemorrhage, infectious exudate, or neoplasm and by which it is stimulated to produce new bone in the early years of life.

Endochondral (intracartilaginous) ossification is prominent in the bones of the appendicular skeleton, the axial skeleton, and the base of the skull. Fundamental to this process is the destruction of cartilaginous tissue derived from the primitive mesenchyme and its subsequent replacement with bone (1,2). The initial sites of this process are designated centers of ossification (primary and secondary), their number and location varying from one bone to another. Although this discussion emphasizes the process of endochondral ossification as seen in a tubular bone, enlarging ossification nuclei are found in other bones as well, including the carpus, tarsus, and bones of the spine.

In tubular bones, the primary ossification center develops in the center of the bone and the secondary center (s), at the ends of the bone, in epiphyses or apophyses, or both. With regard to the primary center of ossification, a central ossific focus develops through a sequence of chondrocyte hypertrophy and death, calcification and vascular invasion, osteoblast transformation, and conversion to bone containing marrow spaces (1). Ossification then proceeds toward the ends of the bone. The migrating frontier of endochondral ossification advancing toward the end of the bone becomes better delineated, eventually forming the growth plate located between the diaphysis and epiphysis of a tubular bone (Fig 1). At the ends of the tubular bones, the same morphologic changes occur, leading to the creation of an enlarging ossification nucleus, the secondary center of ossification. Further maturation leads to the gradual conversion of the secondary ossification center into bone, leaving a subchondral bone plate on the epiphyseal side at the base of the articular cartilage and a physeal scar on the metaphyseal side of the plate. Cartilage remaining at the subchondral surface forms the mature hyaline cartilage that characterizes articular surfaces.

Modeling and Remodeling

Both intramembranous and endochondral ossifications account for longitudinal and radial growth and maturation of the skeleton during childhood and adolescence. Two distinct processes are essential for the sequential developmental modifications that take place in the overall shape, size and strength of bone: skeletal modeling and skeletal remodeling.

Essentials

- The composition of bone matrix can be divided into two types of organization: cortical bone and trabecular bone; these two fractions exhibit considerable differences in their anatomy and biomechanical properties.
- Traumatic insult to bone and cartilage can take the form of a single excessive high-impact force or repetitive below-trauma threshold loads, either of which can cause overload of the tissue resulting in damage.
- The normal biomechanical properties and patterns of failure of cartilage and bone relate to their anatomy and tissue organization, which can be understood at several length scales.

Published online
10.1148/radiol.16142305 **Content code:** MK

Radiology 2016; 280:21–38

Conflicts of interest are listed at the end of this article.

Figure 1

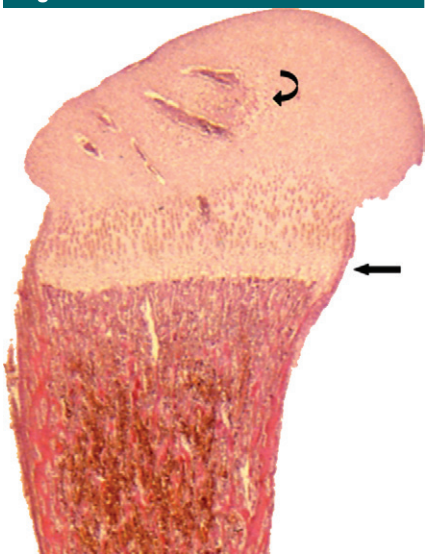

Figure 1: Longitudinal histologic section of a developing proximal femur from a third-trimester fetus illustrating from superior to inferior cartilaginous epiphysis with developing secondary ossification center of the femoral head (curved arrow), the entire growth plate (straight arrow), and the metaphysis and proximal diaphysis containing the primary ossification center.(Hematoxylin-eosin stain, low magnification.)

There are several types of bone cells that differ in origin and function yet communicate with or signal to each other to control and coordinate the processes of modeling and remodeling. The function of one of the cell types, the osteoclast, is unique as its job is to destroy the very tissue that contains it (3). Osteoclasts are derived from mononuclear precursor cells of the monocyte-macrophage lineage (4). Two cytokines, receptor activator of nuclear factor kappa-B ligand, or RANKL, and macrophage colony-stimulating factor, are essential for osteoclast formation, as well as osteoclast survival and organization (4,5). Osteoclasts are responsible for acidification of the resorption compartment, dissolution of the mineral component of the bone matrix, and digestion of the proteinaceous matrix (4,6).

Osteoclastic-induced bone resorption stimulates the release of growth factors that lead to the recruitment of osteoprogenitor precursor cells derived from pluripotent mesenchymal stem cells, which differentiate into osteoblasts. The osteoblasts synthetize new bone matrix by secreting type 1 collagen and other matrix proteins (4). Osteoblasts are found in abundance throughout growing or remodeling bone, whereas in quiescent adult bone, osteoblasts are concentrated on the endosteal cortical surface and in the endosteal tissue that lines the Haversian canals (1).

Osteocytes are long-living, terminally differentiated, nonproliferative cells of osteoblast lineage that constitute the major cell type of mature bone (7). They are trapped within the osteoid material in small lacunar spaces, interconnected by numerous dendritic cytoplasmic processes, and they do not directly secrete matrix or resorb bone (7,8). Osteocytes interact with osteoblasts by releasing molecules that inhibit osteoblast function and bone formation (9). Their secretion of other substances influences the recruitment and function of osteoclasts, signaling osteoclasts that replacement of damaged bone is required (10,11). Through these interactions with osteoblasts and osteoclasts, when bone is damaged osteocytes transmit signals that direct appropriate cellular reaction.

Skeletal modeling leads to changes in the overall shape and size of a bone as a response to the physiologic influences and mechanical forces that are placed upon it (4,12). It is an uncoupled process, in that bone formation and bone resorption are not tightly interdependent, often occurring at different and sometimes distant skeletal sites. Rather, bones widen or narrow, change axes, and develop curvatures through the independent action of osteoblasts and osteoclasts, typically during skeletal growth in childhood. The mechanical and molecular mechanisms accounting for this essential process are only partially understood. Relevant roles are played by systemic regulators, especially hormones, which are influenced by age and sexual maturity (12). The process of skeletal modeling is normally less frequent than that of skeletal remodeling in adults (13–15).

In skeletal remodeling, coupled bone resorption and bone formation occur at the same skeletal site and are chronologically and quantitatively balanced (12). This process begins before birth and continues until death, and it involves the continuous removal of regions of old bone with replacement by newly synthesized proteinaceous matrix and subsequent mineralization of this matrix to form new bone (4). Julius Wolff, a German surgeon and anatomist who lived almost entirely in the 19th century, recognized that bone dynamically remodels in both quantity and architecture to make functional adaptations to changes in loading (16). Although a precise translation of the Wolff law is difficult to find, it is based on the concept that forces or mechanical signals encountered during loading are converted into biochemical stimuli at the cellular level that influence bone remodeling (17,18).

Remodeling occurs in response to increased loading and microscopic damage within cortical osteons or cancellous trabeculae (19). Osteocytes are integral to detection of damage and initiation of the remodeling cycle, but successful remodeling requires the coordinated and synchronized activities of multiple cellular participants that include osteoclasts, osteoblasts, macrophages, and various immune and hematopoietic cells (20). An aggregate of such cells combine to form a microscopic temporary wandering assembly referred to as a basic multicellular unit that targets a discrete area for repair (20,21). The basic multicellular unit is arranged with osteoclasts leading a tail of osteoblasts, forming a cylindrical tunnel known as a cutting cone within cortical bone or an excavation resembling a trench along the trabecular surface in cancellous bone (22). Stages of remodeling include quiescence, activation, resorption, reversal, bone formation, and termination (20) (Fig 2). Normal remodeling progresses slowly, with an entire cycle taking place over a span of several weeks or months.

The basic multicellular unit can be inhibited by factors such as advanced age, chronic illness, drugs, or metabolic

Figure 2

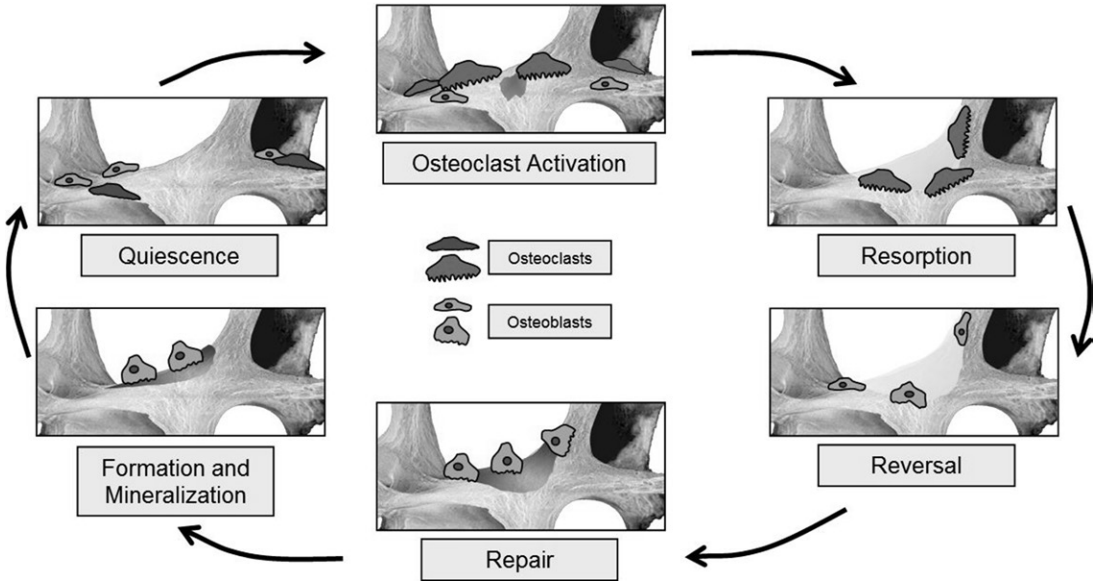

Figure 2: Sequential phases of the normal bone remodeling cycle.

or endocrine dysfunction (23). A recognized consequence of drug-induced basic multicellular unit suppression is the development of atypical fractures of the lateral femoral cortex resulting from prolonged treatment with bisphosphonate alendronate, a potent inhibitor of bone turnover (24) (Fig 3). Bisphosphonates inhibit bone resorption by osteoclast suppression and induction of osteoclast apoptosis, disrupting the bone remodeling cycle. Histologically, the bone surface in patients with atypical femoral fractures is devoid of cellular elements and shows impaired matrix formation, similar to the adynamic bone present in patients with chronic renal failure (23).

Bone Anatomy

Macroscopic Anatomy

The composition of bone matrix can be divided into two types of organization: woven bone and lamellar bone. Woven bone, consisting of an irregular arrangement of collagen fibers that vary in diameter and are not stress-oriented in their direction, is only prominent in fetuses and in situations requiring rapid bone turnover such as during the healing phase of fractures and in disorders such as hyperparathyroidism and Paget disease. The majority of the skeleton in adults is composed of lamellar bone, which is more organized, stronger, and less flexible than woven bone, with collagen orientation that is stress-related. Lamellar architecture is found both in cortical and in cancellous bone, although the precise arrangement of the lamellae varies between the two (1).

The skeleton is composed of both dense compact bone, especially on its surface, known as cortical bone, and a honeycombed framework of plates and struts of bone with intervening spaces, known as cancellous, or trabecular, bone. In adults, cortical bone typically accounts for 80% of the total bone mass, though the exact proportion varies from one person to another and from one anatomic site to another. In the long tubular bones, the peripheral shell of cortical bone is relatively thick, enclosing a central medullary cavity consisting of sparse trabeculae. The intertrabecular spaces contain an admixture of hematopoietic and fatty marrow, the composition varying according to the age and sex of the person, the precise skeletal site, and the hematopoietic demands placed on the skeleton (Fig 4).

Attaching to the surface of many bones are tendons and ligaments, as well as capsular tissue related to nearby articulations, at sites known as entheses (25). It has been suggested that the roughened bone surface markings at tendon insertions indicate that ossification has extended from the bone into the terminal collagen fibers of the tendon, influenced by the strength and direction of pull of the corresponding muscles (1). Ligaments attach directly to the cortical surface or periosteum through fibers that are oriented either perpendicularly or obliquely to the cortex. The anatomic connection between muscle and bone, which influences the tensile stresses placed on that bone, is related not to the direct cortical penetration of muscle fibers but through the connective tissue that encapsulates and pervades these muscles (1).

Microscopic Anatomy

The mineralized extracellular component of bone is designated the matrix, which is composed in part of innumerable collagen fibers that are embedded in a ground substance. The collagen fibers are synthesized by osteoblasts, are intimately associated with the mineral component, and provide structural

Figure 3

Figure 3: Anteroposterior radiograph of the proximal femur in a 78-year-old woman demonstrates a fracture of the lateral cortex of the proximal femur (arrow) related to long-term bisphosphonate use. Note the typical transverse orientation and periosteal beaking associated with these fractures.

Figure 4

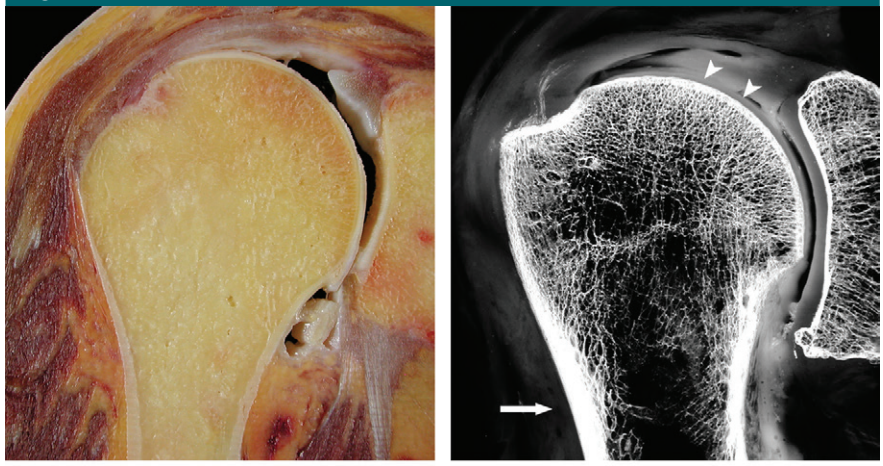

a. **b.**

Figure 4: **(a)** Coronal anatomic section and **(b)** corresponding specimen radiograph of the proximal humerus illustrate the fatty marrow filling the trabecular bone spaces located in the subchondral and medullary regions. Note the thin subchondral bone plate at the humeral head (arrowheads) and the dense cortical bone forming the humeral shaft (arrow).

resistance to biomechanical forces, contributing to the remarkable strength of bone. It is the strength of these collagen fibers more than any other constituent that increases the amount of energy that must be absorbed before a bone will fail. The size and orientation of the collagen fibrils influence the likelihood that microscopic cracks will appear when a bone is stressed and the subsequent magnitude and direction of such cracks as they propagate. The triple helical collagen molecules in bone (most often type I collagen) are aggregated together by innumerable crosslinks. Disruption or cleavage of these crosslinks with aging, trauma, or disease decreases the overall strength of the bone (26,27).

Bone minerals also are a component of the matrix. The major mineral component is hydroxyapatite with small amounts of carbonate, magnesium, and other minerals. These minerals contribute to the strength, rigidity, and hardness of bone and explain its opaque radiographic quality. The mean degree of mineralization of bone is not identical in different skeletal regions, although it is similar in cancellous and cortical bone, between sexes, and at different ages (28). In disorders characterized by increased levels and rates of bone remodeling, there is less time for completion of mineralization, resulting in a lower mean degree of mineralization of bone (27). Conversely, a higher mean degree of mineralization of bone is indicative of a decreased rate of bone turnover. Excessive mineralization of bone does not strengthen the bone; although the bone becomes stiffer, it also is more brittle, reducing the energy required for fracture (29,30). Complicating the issue of the effects of mineralization on overall bone strength is the additional influence of crystal size. Bones with larger crystals, such as osteoporotic bones, are more prone to fail owing to their increased brittleness (27,31).

Articular Cartilage Anatomy

Hyaline articular cartilage is a highly specialized connective tissue that covers the surfaces of those bones that constitute a diathrodial joint. This tissue is hypocellular, aneural, alymphatic, and avascular. It is composed of a small number of cells (chondrocytes) that are located in an extracellular matrix consisting of water and macromolecules that include proteoglycan, collagen, and noncollagenous proteins. The chondrocytes vary in number, size, and shape depending on their location or zone (deep to superficial), and they are responsible for production, organization, and maintenance of the extracellular matrix (32). The complex interaction between the chondrocytes and extracellular matrix maintains structural integrity and confers biomechanical properties to this tissue, including tensile strength and elasticity that facilitate its ability to absorb and distribute load. Structure and function become a part of a feedback loop with chondrocyte biosynthesis guided, at least in part, by stress and strain on the cell (33,34).

Articular cartilage has a zonal configuration consisting of four basic horizontal layers that vary with regard to cellular profile (size, shape, metabolic activity, density), proteoglycan concentration, and collagen organization. These are designated the superficial, transitional, deep, and calcified layers (Fig 5). The superficial layer is the thinnest and is composed of flattened

chondrocytes, proteoglycan (low concentration), collagen (two layers densely packed, with a thin diameter), and water (in the highest concentration of any of the layers) (35). The transitional zone (intermediate or middle) is characterized by round chondrocytes, random collagen organization, and increased proteoglycan concentration. The deep, or radial, zone has the lowest cell volume with a columnar organization of chondrocytes. Here, collagen fibers are oriented perpendicular to the subchondral bone, proteoglycan concentration is high, and water concentration is low. The tidemark, a band of fibrils that serve as an anchor for collagen, separates the deep layer of cartilage from the calcified layer. The calcified zone is characterized by the presence of round chondrocytes and the absence of proteoglycans. It is the transition from and the point of adherence between the superficial cartilage and the subchondral bone (32) (Fig 6).

Figure 5

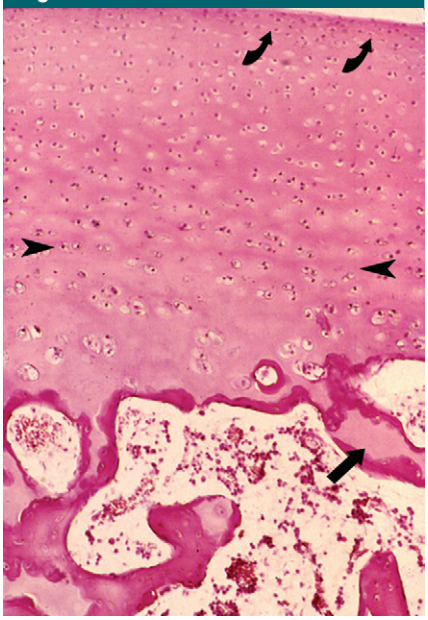

Figure 5: Photomicrograph of normal articular cartilage from a child illustrates the zonal organization of cartilage and the junction of the cartilage with the subchondral bone plate. The approximate boundaries between the thin superficial layer and the transitional layer (curved arrows) as well as between the transitional and deeper radial layers are shown (arrowheads). Note the calcified cartilage (arrow) at the junction of the cartilage and the subchondral bone plate that is still incompletely ossified in this specimen. (Hematoxylin-eosin stain, medium magnification.)

Stresses, Forces, and Modes of Structural Failure

The biomechanical properties of any substance can be described by the relationship between its capacity to absorb load (stress) and its capacity to deform (strain) as force is applied to it. Load refers to the sum of all forces acting on the substance, whereas deformation refers to any change in shape that takes place in that substance as force is applied. This relationship is depicted graphically as a stress-strain (load-deformation) curve (Fig 7), which shows the response of a homogeneous material to external force by illustrating its stiffness (elastic modulus), as well as its yield and failure points (36–38). Materials that can tolerate high loads but are unable to deform, such as glass, are considered brittle, whereas substances that deform considerably before failure are considered ductile. Bone and cartilage behave in an intermediate fashion, able to tolerate moderate stress while also showing the ability to accommodate moderate strain before failure. Any single load-deformation curve is inadequate to describe the inhomogeneous tissue of the human skeleton as there is considerable variation in structure, composition, and geometry in different anatomic regions. Bone itself consists of two distinctly different tissue fractions, with cancellous trabecular bone and cortical bone behaving very differently with the application of force. The skeleton also exhibits anisotropy, responding to stresses differently depending on the direction of loading (37,38). The mechanical properties of bone also vary with age, as bone in the child is more pliable than is adult bone and the cartilaginous physeal plate of immature bone is particularly vulnerable to injury.

Figure 6

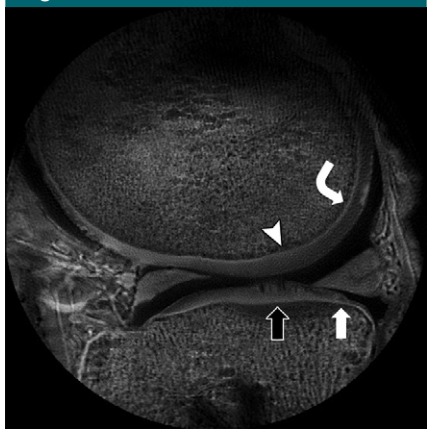

Figure 6: Sagittal ultrashort echo-time (repetition time msec/echo time msec, 500/0.008) magnetic resonance (MR) image of the knee unmasks the short T2 tissue (1-msec T2*) of the normal-appearing calcified layer of femoral (curved arrow) and tibial (white arrow) cartilage and also shows regions of femoral (arrowhead) and tibial (black arrow) calcified cartilage effacement representing degeneration.

Structural loading may be uniaxial, in which the force is applied to a substance in only one direction, or it may be multiaxial, in which the force is geometrically more complex, with stress applied to the substance in two or more directions (38) (Fig 8). Compression, tension, and shear forces are forms of uniaxial loading. In simple terms, compressive stresses develop when applied forces act to reduce the length of a material in the axis of the applied load, and tensile stresses develop when applied forces act to lengthen a material along the axis of the applied load. Shear stresses act to separate one layer of a material from an adjacent one in a single plane. Buckling is a mode of failure characteristic in a long slender column when compressive forces are applied at the long ends, leading to lateral deflection of a structure. The magnitude of the force that leads to buckling is less than the maximal compressive force that the material can bear and is described mathematically by Euler law (39).

Multiaxial loading of a substance occurs when force is applied in two or more planes simultaneously. Typical examples of multiaxial loading include bending and torsion (rotation). Bending results in one side of the substance experiencing compression and the other

side of the substance experiencing tension, leading to deflection, sagging, or sideways movement of a material. Torsion occurs when one end of a substance is rotated in one direction and the other end remains motionless or rotated in the opposite direction, resulting in twisting of the material, leading to internal shear stresses in the material. More complex forms of force application are recognized but are beyond the scope of this article. Furthermore, there may be a combination of several different types of stress applied simultaneously, adding to the complexity of analyzing skeletal biomechanics during normal loading, overloading, and injury (37,38).

Figure 7

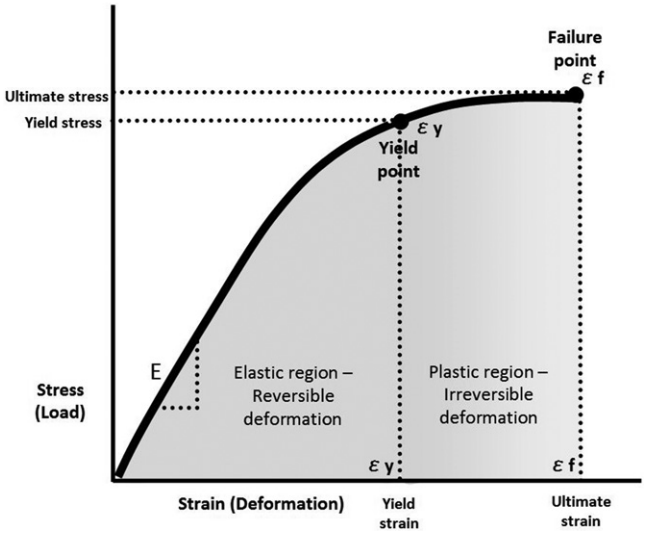

Figure 7: The stress-strain curve for any material illustrates the relationship between the amount of load it can absorb and the deformation it can tolerate before reaching its yield point and ultimately its failure point. The slope of the curve (ε) is defined as the elastic modulus for that material.

Chondral and Osteochondral Injury

The biomechanical behavior of articular cartilage is determined by the interaction of its predominant components: collagen, proteoglycan, and interstitial fluid. Collagen fiber networks contribute to joint mechanics directly by resisting tensile stresses and indirectly by augmenting pore fluid pressure (40). In cartilage matrix, the volume occupied by the proteoglycan aggregate is limited by the collagen network. With compression, the negatively charged components of the proteoglycans are pushed closer together, increasing their repulsive forces and adding to the compressive stiffness of cartilage. Damage to the collagen framework reduces compressive stiffness of the tissue as the proteoglycans are contained less efficiently. With chondral deformation, fluid flows through the tissue and across the articular surface, producing a thin film that lubricates that surface and contributes to effective joint motion (41,42). The recognition that fluid flow and deformation of tissue are interdependent underscores the concept that cartilage can be considered a biphasic mixture of both fluid and solid

Figure 8

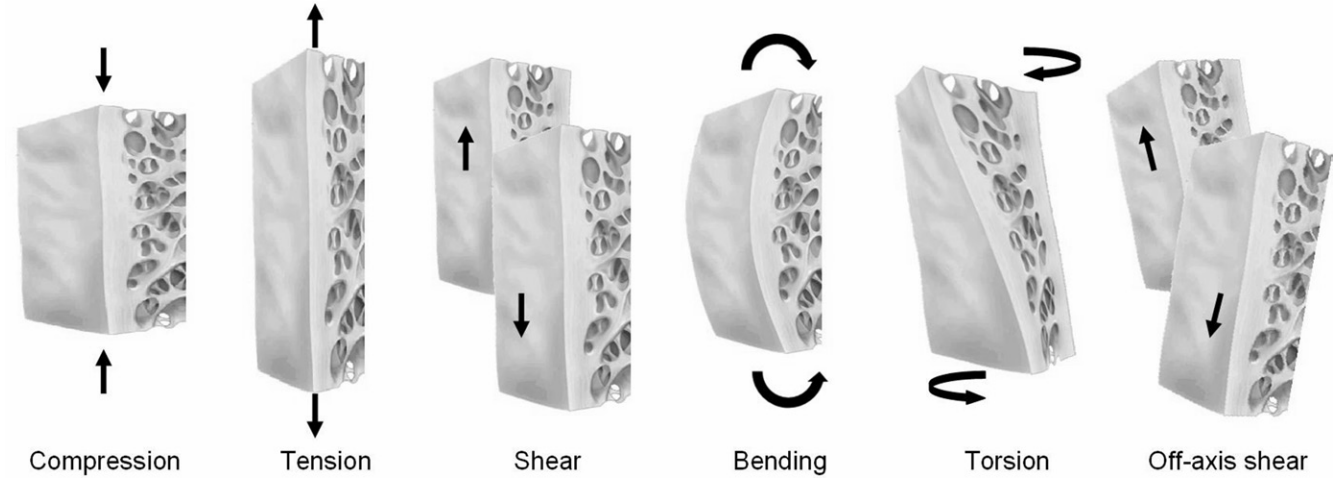

Figure 8: The principal mechanisms of injury of bone and cartilage are illustrated. Compression, tension, and shear are uniaxial mechanisms, whereas bending, rotation, and off-axis shear are more complex, with force applied in two or more planes.

Figure 9

Figure 9: Sagittal intermediate-weighted (2000/20) MR image of the knee demonstrates a full-thickness chondral fissure (arrow) in the patellar cartilage.

Figure 10

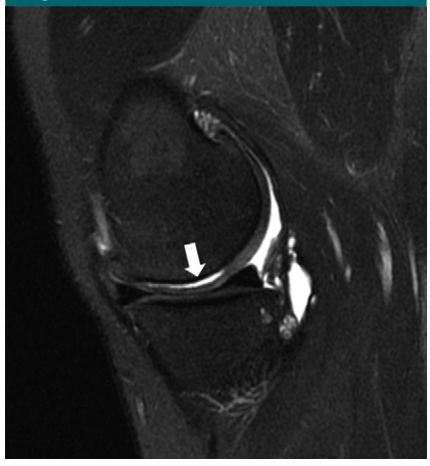

Figure 10: Sagittal T2-weighted fat-suppressed (3200/65) MR image of the knee shows separation of the femoral articular cartilage from the subchondral bone (arrow), with no demonstrable extension to the surface of the articular cartilage. This abnormality represents a concealed (not visible at arthroscopy) delamination of the cartilage from the underlying bone.

Figure 11

Figure 11: Sagittal T2-weighted fat-suppressed (3200/65) MR image of the knee demonstrates a focal full-thickness chondral defect (arrow) of the femoral condyle, representing a grade 4 Outerbridge lesion. Its narrow zone of transition with the adjacent cartilage supports a posttraumatic etiology.

components, with material properties that include stiffness and permeability (41).

Chondral and osteochondral injuries are commonly encountered, particularly in the lower extremity due to either a single excessive high-impact force or repetitive subthreshold loads. Resulting structural alteration includes three types of cartilage injury: chondral damage without visible tissue disruption (cartilage at risk), disruption of articular cartilage alone, and disruption of articular cartilage and subchondral bone together (osteochondral injury). The precise role of trauma in the development of osteoarthrosis, a finding seen in more than 60% of adult knee arthroscopies, is unclear (43–45).

In the setting of acute trauma, injury is related to one of three types of force: compression, shear, or tension (46,47). Compression forces are applied perpendicular to the joint surface, inducing nonuniform deformation of articular cartilage. The spatial profile and the magnitude of the deformation depend on a number of variables, including the magnitude and rate of loading, joint geometry, and the mechanical properties of the tissue (48). Spatially, the greatest deformation occurs at the contact point superficially and diminishes toward the deep layer (49). The rate of loading also influences the degree of cartilage deformation (50,51). With high rates of loading, the relatively stiff cartilage dissipates energy within its superficial region, producing superficial fissures (52,53) (Fig 9). Lower rates of loading result in energy transferred to the deeper layers of the tissue, producing focal regions of chondral loss. Compressive strain as low as 30% can result in cell death if the strain rate is sufficiently high (54,55). As the magnitude of the force increases, chondrocyte viability decreases and cartilage lesions of progressive severity develop (> 50%) (56–59). Of note, even in the absence of visible structural damage, cell death and matrix injury may result from compression, producing a "cartilage-at-risk" scenario that ultimately leads to tissue compromise (60–64).

Shear forces are applied parallel to the joint surface. The speed and energy of shear force will influence the pattern and extent of cartilage failure, leading to chondral delamination injuries that vary with regard to the zone of cartilage that is involved and the presence or absence of violation of the cartilage surface (65). Excessive shear force can produce surface-layer tears of cartilage along obliquely oriented fibers in the transitional zone or, when transmitted to the osteochondral junction, can debond the calcified layer of cartilage from the underlying bone plate (53) (Fig 10). Tensile forces characteristically lead to avulsive injuries, where ligaments or tendons exert traction at their osseous attachments rather than cartilage damage. Osteochondral injuries involve both cartilage and subchondral bone and may be acute, subacute, or chronic, with those abnormalities of longer duration being designated osteochondritis dissecans (66).

In the clinical assessment of chondral and osteochondral injuries, the size and depth of the lesion, its location, and any associated involvement of the subchondral bone must be considered. A common clinical classification system used for the description of articular cartilage abnormality is that of Outerbridge (67), in which articular cartilage damage varies among four grades based on the depth of the chondral abnormality (68) (Fig 11). The accuracy and reproducibility of this system have been reported to range from 22% to 100%,

Figure 12

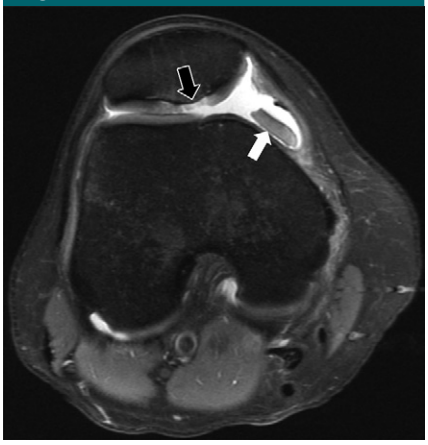

Figure 12: Axial intermediate-weighted fat-suppressed (2400/24) MR image of the knee shows an osteochondral injury (black arrow) at the median ridge of the patella with associated bone marrow edema. A shed fragment (white arrow) with linear low signal intensity at its edge represents a portion of the attached subchondral bone plate.

Figure 13

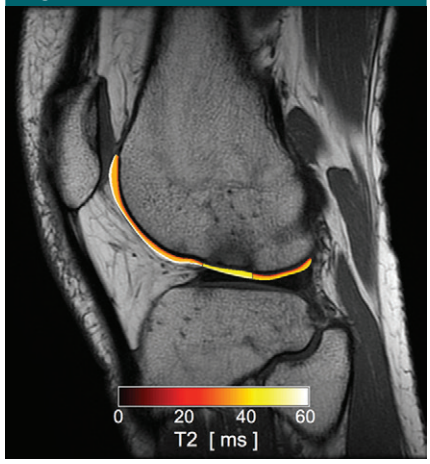

Figure 13: Sagittal intermediate-weighted (1800/20) MR image in a patient after an anterior cruciate ligament tear with superimposed T2 color map on the lateral femoral articular cartilage shows focal increased T2 value of the condylopatellar sulcus cartilage in the region of bone marrow contusion. While no chondral loss is noted, the altered T2 values represent alteration in the collagen infrastructure of the tissue.

lower grade lesions being diagnosed with less accuracy than higher grade lesions (69). More recently, the Modified International Cartilage Repair Society Chondral Injury Classification System has gained acceptance (70). This latter system focuses on lesion depth (graded from 0 to 4) and the area of damage (graded from normal to severely abnormal). The International Cartilage Repair Society has also developed a classification system for osteochondral injuries based on the size, depth, and stability of the abnormality (71).

The assessment and grading of chondral and osteochondral injuries by using MR imaging are straightforward when true morphologic alterations are present. In the setting of higher grade acute injury, the signal alteration in the articular cartilage is readily visible and frequently associated with altered signal intensity in the adjacent subchondral bone marrow and displaced cartilage (Fig 12). However, low-grade chondral injury typically involves very little morphologic change. Traditional grading systems have classically used altered T2 signal within the cartilage to infer the presence of infrastructural damage (72–74). The development of quantitative MR techniques provides direct evaluation of tissue biochemistry in the setting of injury. Several techniques are available to assess the integrity of cartilage glycosaminoglycan, including sodium MR imaging, delayed gadolinium-enhanced MR imaging of cartilage, and T1 ρ imaging (75–78). To assess collagen orientation, quantitative T2 mapping is most often utilized (79) (Fig 13).

Subchondral Bone

Anatomic and Biomechanical Considerations

Just beneath the calcified zone of articular cartilage exists a layer of compact bone designated the subchondral bone plate that serves to separate the articular cartilage and subchondral trabeculae. The thickness of the subchondral bone plate varies both within and between bones (80). Its shape generally follows that of the articular surface of the specific bone of which it is a part, and it represents an important component of the support system that responds to and resists the forces placed on the articular surface, forces that vary as the joint moves (81,82). Those stresses within the subchondral bone plate are transmitted, in part, to the trabeculae that lie beneath it. Indeed, some investigators have reported that the subchondral bone plate and adjacent trabeculae absorb most of the mechanical forces transmitted across the joint (81).

Normal trabecular architecture varies from one anatomic site to another, consisting in part of groups of linear or arc-like trabeculae that, in most sites, are thickened and oriented along the axes of the major compressive and tensile stresses within that bone (83). Many trabeculae in frequently compressed regions of the joint are oriented at nearly right angles to the subchondral bone plate, extending downward into the parent bone for variable distances. Elsewhere, the trabeculae are obliquely oriented. Crossing trabeculae intersect these vertical and oblique trabeculae, mainly in an orthogonal pattern (84–87) (Fig 14). Chambers are created in the subchondral cancellous bone consisting of central areas containing regions of marrow and peripheral walls composed of these trabeculae. The size and shape of these chambers vary from one bone to another and in different regions of a single bone.

The most extensively studied trabeculae in the human body are those located in the femoral head and neck, where five major trabecular groups are identified: principle compressive, principle tensile, secondary compressive, secondary tensile, and greater trochanteric groups (88–90) (Fig 15). The Singh index, historically used to judge the presence and degree of osteoporosis, was based on the morphology of these trabecular groups (91). Unfortunately, the proximal femur is a particularly challenging region due to the number and complexity of the trabecular groups and their complex relationships with the cortex and calcar. At least some of the trabecular intersections in the femoral head and neck are not orthogonal, and the trabecular orientations do not necessarily correspond

Figure 14

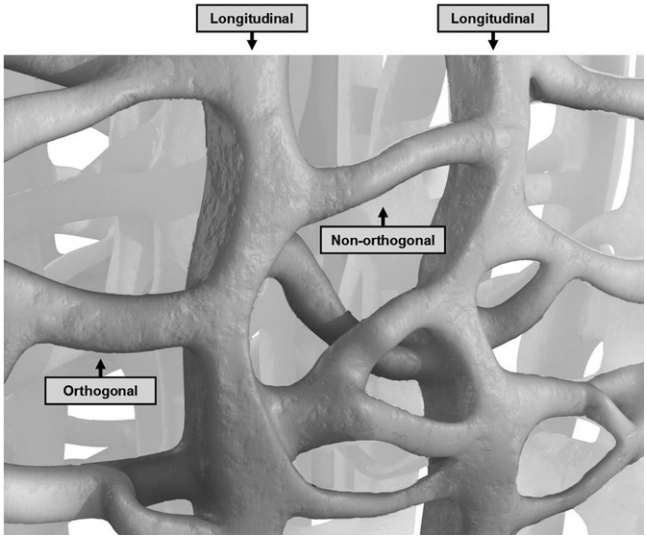

Figure 14: Graphic representation of trabecular organization illustrates the thicker longitudinal trabeculae bridged by transverse trabeculae at varying angles. (Modified, with permission, from Marion Karl, Lure Animations, Reno, Nev.)

Figure 15

Figure 15: High-resolution 0.9-mm-thick coronal MR image of a proximal femur specimen obtained with a three-dimensional spin-echo sequence demonstrates the trabecular pattern of the proximal femur. (Courtesy of Thomas Link, MD, UCSF, San Francisco, Calif.)

Figure 16

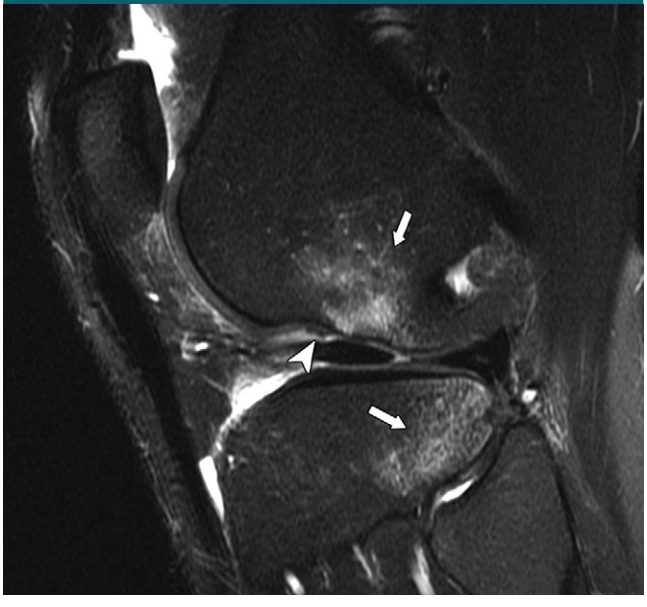

Figure 16: Sagittal intermediate-weighted fat-suppressed (2400/26) MR image of the knee in woman with an acute anterior cruciate ligament tear shows marrow edema in the distal femur and proximal tibia (arrows). There is an osteochondral impaction fracture at the femur with a deepened lateral notch sign (arrowhead). The tibial edema is related to a contusion, without overlying chondral or osseous disruption.

to the directions of the principle stress directions of any one loading condition (88,92,93).

Subchondral Contusion (Bone Bruise)

With the development of MR imaging came the discovery that alterations in marrow signal could result from injury even in the absence of a visible fracture, a phenomenon designated a bone contusion, or bone bruise (94). The distribution of bone contusions varies according to the mechanism of injury, some distributions being characteristic of injury to a specific ligament, such as the anterior cruciate (95) (Fig 16). Compressive forces placed on the articular surface are transmitted through the cartilage to the subchondral trabeculae that fail and develop microfractures as they buckle under the load. Conceptually, accompanying this process or acting independently, hemorrhage and edema within the trabecular chambers could "pressurize" the marrow, thereby increasing the tensile stress on the walls of that chamber. This response is analogous to a compressed automobile tire in which a load applied to its top and bottom pressurizes the air within, which itself places greater tensile stress on its side walls. Similar mechanisms have been invoked to explain the appearance of enlarging subchondral bone cysts, especially in osteoarthrosis (96).

Few reports exist regarding the histologic alterations that characterize a bone contusion, although Rangger and colleagues (97) found microfractures of cancellous bone and marrow edema and hemorrhage in a histologic study

of bone bruises of the knee in a small group of patients, the specimens provided by means of either arthroscopy or postmortem examination. A recent study has emphasized another form of bone contusion that has a distinctive appearance on MR images related to liquefied and necrotic fat within or adjacent to an osseous injury, sometimes surrounded by what appears to be an inflammatory reaction (98) (Fig 17). The fat "globules" may migrate from one chamber to the next as the trabecular walls are breached by the injury. It is not known whether such foci of liquefied fat contribute to systemic fat embolization recognized following major skeletal injury (99).

Figure 17

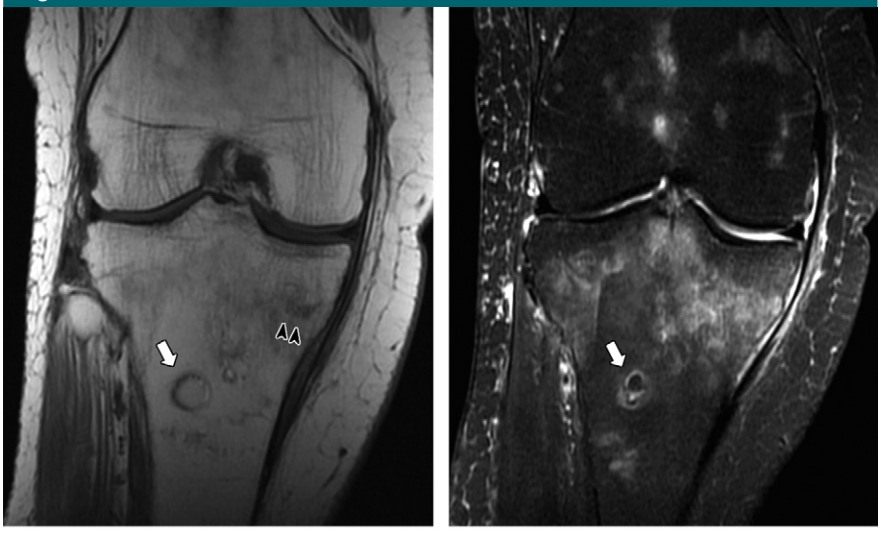

a. b.

Figure 17: **(a)** Coronal T1-weighted (600/20) and **(b)** intermediate-weighted fat-suppressed (3100/35) MR images of the knee in an elderly woman with an insufficiency fracture (arrowheads) of the medial tibial plateau related to osteoporosis demonstrate globular collections (arrow) of marrow fat adjacent to the fracture.

Cortical Bone

Biomechanics of Cortical Bone

Cortical bone differs considerably from cancellous bone in its anatomic distribution, as well as in its composition and architecture. The difference in density between cortical bone and trabecular bone is the major factor accounting for the different biomechanical properties of these two tissues (100). Cortical bone is compact and dense, with a porosity of 5%–10% as compared with the loose trabecular architecture of cancellous bone in which 50%–90% porosity is typical (101) (Fig 18). Bone loss related to aging increases cortical porosity, decreasing its strength and increasing the risk of fracture, primarily by diminishing the

Figure 18

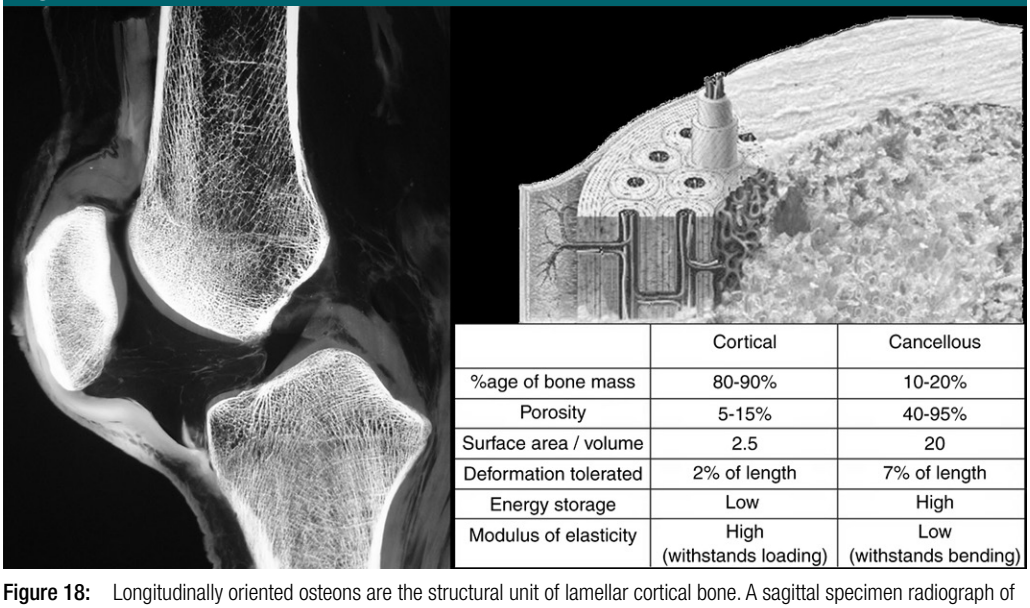

	Cortical	Cancellous
%age of bone mass	80-90%	10-20%
Porosity	5-15%	40-95%
Surface area / volume	2.5	20
Deformation tolerated	2% of length	7% of length
Energy storage	Low	High
Modulus of elasticity	High (withstands loading)	Low (withstands bending)

Figure 18: Longitudinally oriented osteons are the structural unit of lamellar cortical bone. A sagittal specimen radiograph of the knee illustrates the difference in appearance between the dense peripheral cortical bone and the porous trabecular bone in the medullary space and subchondral region. The biomechanical differences between these two bone fractions are shown in the accompanying chart.

Figure 19

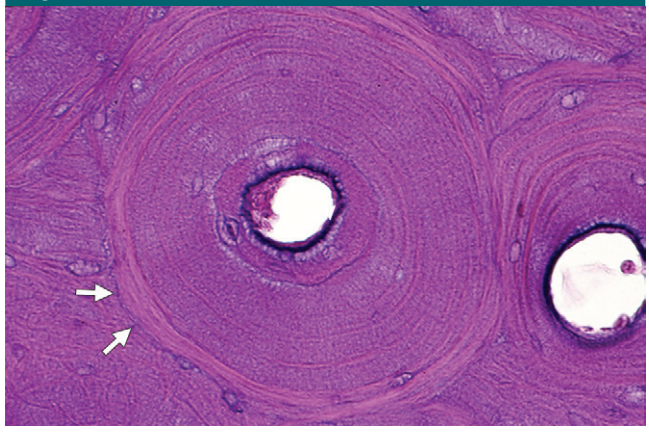

Figure 19: One complete cross-section and one partial cross-section of cortical osteons illustrate the central Haversian canals surrounded by concentric lamellae. A thin cement line (arrows) is visible at the margins of the complete osteon. Interstitial lamellae are noted outside these two osteons. (Hematoxylin-eosin stain, medium magnification.)

capacity of the cortex to tolerate stress (102). Cortical bone is stronger and has a higher capacity for load absorption, particularly in compression, than cancellous bone but it exhibits a higher modulus of elasticity, indicating it is stiffer and less flexible than cancellous bone, which can deform three to four times to a greater extent (38).

Cortical bone microstructure is similar to that of cartilage and other fiber-reinforced composite materials, whereby the brittle mineralized elements are reinforced and strengthened by the ductile collagenous components (36). Osteons are its basic structural unit, having a characteristic arrangement known as a Haversian system, with concentric cylinders of mineralized bone matrix that surround a central area containing neurovascular channels designated Haversian canals. There are approximately 21 million osteons in the adult skeleton, averaging 400 μm in length and varying from 100 to 400 μm in diameter (1,4). Microscopically, osteons are arranged in parallel bundles along the long axis of the shaft, with interstitial lamellae located between adjacent osteons. At the junction of the osteon and the interstitial lamellae, cement lines are deposited (Fig 19). The cement line has been regarded as an area with decreased mineralization, potentially important in the initiation and deflection of cortical cracks (103,104).

Cortical bone is located predominantly in the shafts of the long bones, with lesser amounts located as a thin external shell surrounding the cancellous bone of the flat and irregular bones. The diaphysis of the long tubular bones is arranged as a peripheral ring of dense cortical bone that encircles a porous central medullary space. This tubular shape, analogous to a hollow cylinder, is optimal for withstanding the many external and internal forces imposed on the shaft as a hollow cylinder, when considered by weight, is far stronger than a solid material (105). The strength of the shaft increases as its outer diameter and/or its wall thickness increase, with differences in these properties alone accounting for more than 55% of the variance in cortical bone strength (26).

Crack Initiation and Deflection

Cortical bone fractures can be caused by either the application of a single high-amplitude force (traumatic fracture), a subthreshold force applied to bone weakened from a pathologic process such as a neoplasm (pathologic fracture), or accumulative microdamage related to repetitive injury (stress fracture) (106). Cortical bone patterns of failure relate to its hierarchical organization, which can be understood at the microscopic scale, in which collagen delamination, microdamage, and microcracking develop, and at the macroscopic scale, in which clinically important fractures are encountered (107,108) (Fig 20). Crack initiation in cortical bone typically takes place on or near its surface. The morphology of the microcrack varies according to the mechanism of loading, with compressive cracks being longer and angulated 30°–40° relative to the cortex and tensile cracks being smaller and oriented perpendicular to the tensile force. While tensile cracks can cause more diffuse damage, subsequent propagation to a frank fracture is more common with compressive injury (19).

Bone-toughening mechanisms such as crack deflection and crack bridging by collagen attempt to contain damage within the cortex and prevent the propagation of a microscopic crack to a macroscopic fracture (106,107,109,110). At low levels of force, transverse microcrack propagation within the cortex is inhibited by the concentric lamellar arrangement of mineralized collagen within the osteon, as well as the cement lines located on the surfaces of the tightly packed osteons (111,112). These longitudinally oriented interfaces inhibit transverse crack propagation, resulting in longitudinal deflection and tortuous crack pathways as the crack is deflected over and over again at these boundary interfaces (109) (Fig 21). At high levels of force, the toughening mechanisms are overwhelmed and microcracks propagate transversely across the entire cortex resulting in a frank fracture.

While longitudinally oriented cracks in the cortex are common at the microscopic level (109), macroscopic longitudinal cortical fractures are uncommon in clinical practice, particularly following a single episode of trauma. This unusual fracture pattern is more typically the result of repetitive stress, observed most commonly in the tibia, followed by the femur, fibula, humerus, and patella (113–115).

Figure 20

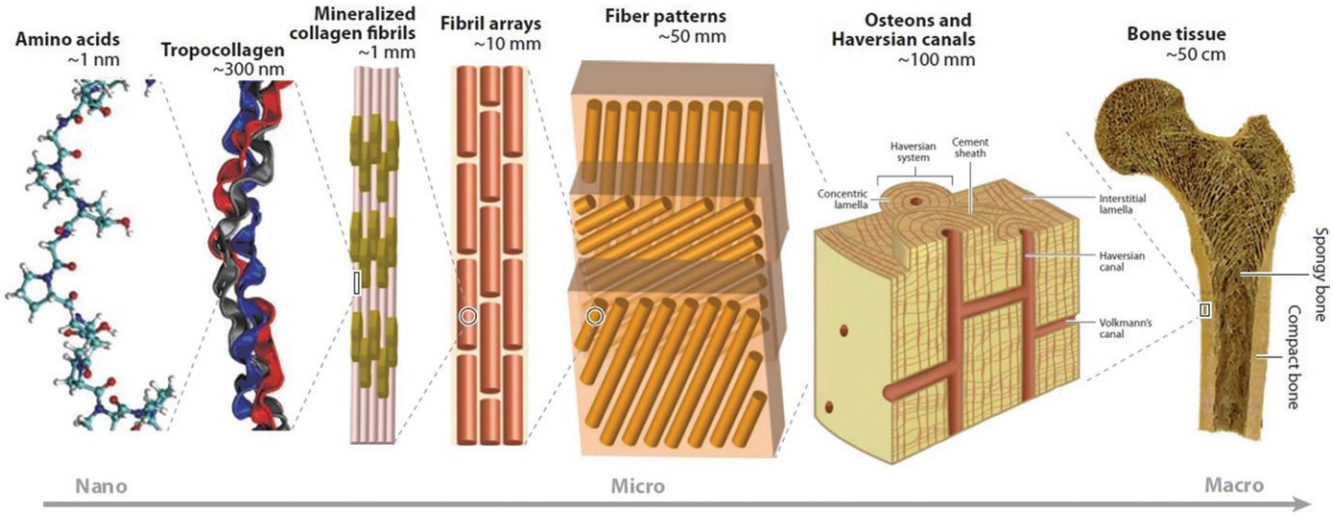

Figure 20: A hierarchical scale model of cortical bone shows the various length scales of the tissues that make up the cortex. The osteon is the basic structural unit of cortical bone. (Modified and reprinted, with permission, from reference 108.)

Figure 21

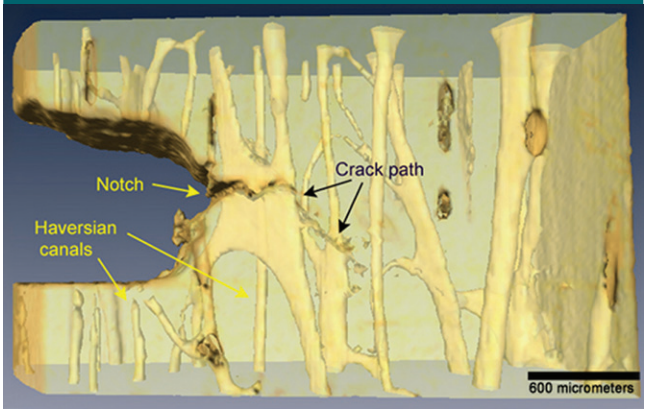

Figure 21: The crack pathway from a notch created in a cortical bone specimen, showing crack deflections related to longitudinal boundaries created by cement lines and bone lamellae. (Modified and reprinted, with permission, from reference 109.)

Cortical Fracture

A traumatic fracture of cortical bone results from the sudden application of a load that exceeds its stress and/or strain threshold, with the orientation of the fracture line reflecting the geometric orientation of the force applied to the bone surface (100). Compression of the bone, as seen after landing from a fall, results in a vertical fracture, although the shaft of the bone rarely fails under compression unless there is an additional angular force (36). Rather, compressive failure typically occurs in the cancellous trabeculae that dominate at the end of the bone. Tensile injury of the bone classically results in an avulsion fracture at an enthesis; such attachments are concentrated at the bone ends. Multiaxial mechanisms of injury such as bending and torsion result in most shaft fractures, with bending causing transverse or short oblique fractures and torsion resulting in spiral fractures in the shaft of the bone (36,116,117). These patterns of fracture are frequently seen in the tibia and fibula following twisting injuries of the ankle. Bending initially results in transverse crack formation in the tensile side of bone, although most traumatic fractures attributed to bending are actually the result of a combination of bending and axial loading, resulting in tensile failure of the convex side and shearing failure on the compressive side, creating an oblique fracture line (36,38). Simultaneous application of force by a combination of these mechanisms occurs frequently, resulting in complex fractures that show features reflecting more than one simple fracture pattern (Fig 22).

Direct force applied to bone is a less common cause of a traumatic fracture than indirect force. Direct force of low magnitude, such as being struck by a low-velocity object such as a fist, results in a transverse fracture at the site of force application, as seen with the nightstick fracture of the ulna. Direct force of a higher magnitude, such as being hit by a moving vehicle, results in a more complex fracture pattern typically associated with comminution (37,117).

Stress Injury of Bone

Stress injury of bone encompasses a spectrum of abnormalities that occur when bone is exposed to repetitive loading, with each load event itself below

Figure 22

Figure 22: Anteroposterior radiograph of the right tibia and fibula demonstrates a comminuted tibial fracture with a butterfly fragment (arrow) and a transverse distal fibular shaft fracture. Note the comminution, displacement, and angular deformity of the fractures, indicating complex forces were applied to them during the injury.

the failure threshold of bone (118). Unlike a traumatic fracture, in which bone fails due to a single episode of loading, stress injury occurs due to a cumulative imbalance between the development of microdamage and the capacity of the bone to repair itself. Stress injury results in numerous forms of disruption of the bone remodeling cycle that are imprecisely defined and not clearly separable, leading to confusion in the terminology and the grading of these injuries (118,119). A stress fracture is the end point of a continuous spectrum of morphologic alterations that range from asymptomatic remodeling through various stages of stress-related alterations in bone architecture, including microdamage, microcrack formation and propagation, focal bone resorption, and macrofracture (120).

Stress fractures are traditionally divided into insufficiency and fatigue subtypes. Insufficiency fractures result from repetitive stresses within the normal range of activities applied to bone that itself is abnormal, whereas fatigue fractures are the result of repetitive excess stress applied to normal bone. The fatigue form is classically seen in young persons, especially those involved in athletic endeavors. Insufficiency injuries are typically associated with metabolic bone diseases, such as osteoporosis, and usually occur in persons older than those with fatigue injuries (120). There are however many persons whose stress injury does not fit neatly into the fatigue or insufficiency category but rather has components of both. With the current emphasis on maintaining good health and "staying in shape," middle-aged and elderly persons are more likely to participate in vigorous exercise and recreational sports, explaining the increasing frequency of fatigue failure of bone in the older population. Conversely, the presence of nutritional or metabolic disorders in the young can result in inadequate bone strength and the development of insufficiency fractures. A classic example of the latter situation is the "female athlete triad," a syndrome of three overlapping conditions that include energy deficiency with or without disordered eating, menstrual disturbance, and bone mineral loss. The presence of one or more components of this triad increases the risk for stress fracture in the young female athlete (111,120).

Insufficiency Fracture

There exists a whole range of abnormalities that can weaken the bone itself, related to diminished mineralization, decreased bone strength and toughness, loss of elastic resistance, or deficient bone architecture, or combinations of these, or alternatively, related to a breakdown in the normal mechanisms of bone repair (26,108,112). In clinical practice, osteoporosis, osteomalacia, and prior bone irradiation are the most common disorders that result in deficiency in the capacity of the bone to sustain routine loading (112). While osteoporosis is generally considered to be the leading cause for insufficiency injury of bone, measurements of bone mineral density alone explain only 70%–75% of the variance in bone strength (121).

Metabolic bone disorders preferentially affect cancellous bone, which has a 10-fold higher proportion of surface area to mass than cortical bone, exposing large amounts of this surface to metabolic stimuli and regional blood flow. The bone loss seen in the cancellous trabeculae is nonuniform, with preferential loss of the secondary trabeculae rather than the primary longitudinally oriented weight-bearing trabeculae, leading to disordered bone architecture that fails easily with even physiologic loading (121). The ability of the unsupported primary longitudinal trabeculae to absorb compressive loading is severely diminished due to the loss of supporting secondary trabeculae, resulting in buckling failure as predicted by Euler law. Buckling failure of contiguous primary trabeculae accounts for the typical orientation of insufficiency fractures, which propagate perpendicular to the axis of the primary trabeculae.

Insufficiency fractures typically affect those regions of bone where there is a high cancellous fraction, such as the vertebral bodies, the flat bones of the pelvis (particularly the regions of the sacral ala), the subchondral regions of the long tubular bones, and the small irregular bones of the foot (such as the calcaneus). Collapse of the subchondral bone leads to an imaging appearance that simulates that of osteonecrosis. As an example of this, overloading of the subchondral bone about the knee, typically accompanied by adjacent meniscal and chondral abnormalities, results in collapse at the

Figure 23

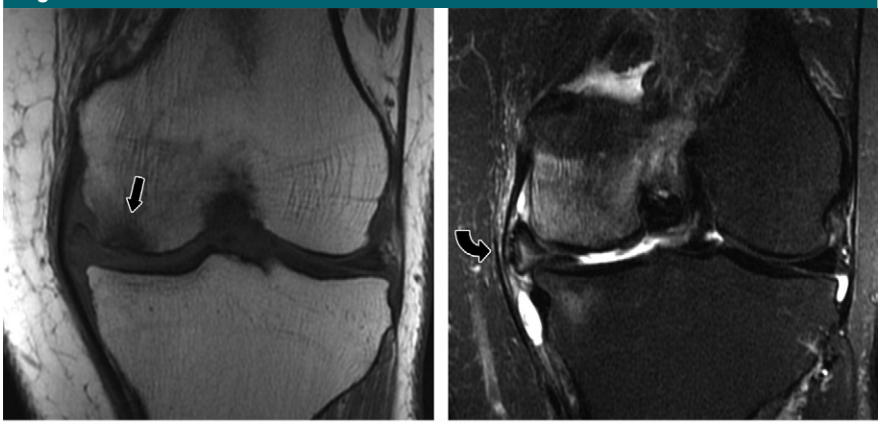

a. b.

Figure 23: **(a)** Coronal T1-weighted (600/20) and **(b)** intermediate-weighted fat-suppressed (3100/30) MR images of the knee in a middle-aged woman with a subchondral insufficiency fracture of the medial femoral condyle (straight arrow) with secondary collapse of the weight-bearing surface. There is peripheral meniscal extrusion (curved arrow) related to a tear of the posterior root of the meniscus (not illustrated), resulting in mechanical overload of the overlying bone and cartilage. Note the chondral loss at the medial femur and the intense marrow edema in the area of the fracture, as well as an effusion and fluid distending the tibial collateral bursa within the medial collateral ligament.

Figure 24

a. b.

Figure 24: **(a)** Anteroposterior radiograph and **(b)** coronal intermediate-weighted (3100/35) fat-suppressed MR image in a runner with left hip pain demonstrate a fatigue fracture of the femoral neck (arrow) located on the medial (compressive) side of the femoral neck.

subchondral bone plate of the femur or tibia, a condition previously and erroneously designated spontaneous osteonecrosis (122) (Fig 23).

Fatigue Fracture

Fatigue injury of bone is most frequently encountered in the cortical bone in the lower extremities, particularly in the second and third metatarsal necks, the middle and distal shaft of the tibia, and the femoral neck adjacent to the lesser trochanter near the junction of the shaft and the femoral calcar (Fig 24). The role of muscle activity in generating compressive, shear, and torque forces on bone has been emphasized in previous descriptions of fatigue fractures, suggesting that an imbalance between bone strength and muscle strength contributes to the development of such injuries (123). Fatigue injury in cortical bone initially takes the form of microcracks at the bone surface. These can be identified histologically and with techniques such as high-resolution microcomputed tomography (121), but they are not visible with routine imaging methods until they are extensive enough to incite a periosteal response. As the injury progresses, longitudinal deflection of microcracks results in intracortical resorption cavities of variable size and orientation, producing radiolucent regions and, ultimately, reactive marrow edema as the damage approaches the medullary space (119). Progression of stress injury results in extension of these intracortical microfractures to the endosteal cortex and, ultimately, to the development of a transversely oriented frank fracture line that enters the medullary space.

Summary

In conclusion, knowledge of the macroscopic and microscopic anatomy, as well as the basic biomechanics, of bone and cartilage provides the foundation for a better understanding of the manner in which this tissue responds to altered mechanical forces and sheds light on the imaging appearances associated with both acute and repetitive injury.

Acknowledgments: We thank Parvis Haghighi, MD, Professor of clinical pathology at UCSD and Director of anatomic pathology at the VA Medical Center San Diego for providing the histology material, Won Bae, PhD, Research Scientist, UCSD MSK Imaging Research Laboratory for reviewing the biomechanics portions of this manuscript, and Deborah Trudell, RT, for preparing the anatomic sections.

Disclosures of Conflicts of Interest: M.N.P. disclosed no relevant relationships. **C.B.C.** disclosed no relevant relationships. **D.L.R.** disclosed no relevant relationships.

References

1. Standring S. Functional anatomy of the musculoskeletal system. In: Standring S, ed. Gray's anatomy: the anatomical basis of clinical practice. 40th ed. Philadelphia, Pa: Churchill Livingstone Elsevier, 2008; 81–97.

2. Kini U, Nandeesh BN. Physiology of bone formation, remodeling, and metabolism. In: Fogelman I, Gnanesegaran G, van der Wall H, eds. Radionuclide and hybrid bone imaging. Berlin, Germany: Springer-Verlag, 2012; 29–57.

3. Karsenty G, Oury F. Biology without walls: the novel endocrinology of bone. Annu Rev Physiol 2012;74:87–105.

4. Clarke B. Normal bone anatomy and physiology. Clin J Am Soc Nephrol 2008;3(Suppl 3): S131–S139.

5. Xiong J, O'Brien CA. Osteocyte RANKL: new insights into the control of bone remodeling. J Bone Miner Res 2012;27(3):499–505.

6. Boyle WJ, Simonet WS, Lacey DL. Osteoclast differentiation and activation. Nature 2003;423(6937):337–342.

7. Kogianni G, Noble BS. The biology of osteocytes. Curr Osteoporos Rep 2007;5(2):81–86.

8. van der Plas A, Aarden EM, Feijen JH, et al. Characteristics and properties of osteocytes in culture. J Bone Miner Res 1994;9(11): 1697–1704.

9. van Bezooijen RL, ten Dijke P, Papapoulos SE, Löwik CW. SOST/sclerostin, an osteocyte-derived negative regulator of bone formation. Cytokine Growth Factor Rev 2005;16(3):319–327.

10. Noble BS. The osteocyte lineage. Arch Biochem Biophys 2008;473(2):106–111.

11. Marie PJ. Bone remodeling: a social network of cells. Medicographia 2012;34:149–154.

12. Teti A. Bone development: overview of bone cells and signaling. Curr Osteoporos Rep 2011;9(4):264–273.

13. Kobayashi S, Takahashi HE, Ito A, et al. Trabecular minimodeling in human iliac bone. Bone 2003;32(2):163–169.

14. Ubara Y, Fushimi T, Tagami T, et al. Histomorphometric features of bone in patients with primary and secondary hypoparathyroidism. Kidney Int 2003;63(5):1809–1816.

15. Ubara Y, Tagami T, Nakanishi S, et al. Significance of minimodeling in dialysis patients with adynamic bone disease. Kidney Int 2005;68(2):833–839.

16. Wolff J. The classic: on the inner architecture of bones and its importance for bone growth. 1870. Clin Orthop Relat Res 2010;468(4):1056–1065.

17. Duncan RL, Turner CH. Mechanotransduction and the functional response of bone to mechanical strain. Calcif Tissue Int 1995;57(5):344–358.

18. Frost HM. A 2003 update of bone physiology and Wolff's Law for clinicians. Angle Orthod 2004;74(1):3–15.

19. Chapurlat RD, Delmas PD. Bone microdamage: a clinical perspective. Osteoporos Int 2009;20(8):1299–1308.

20. Raggatt LJ, Partridge NC. Cellular and molecular mechanisms of bone remodeling. J Biol Chem 2010;285(33):25103–25108.

21. Ott SM. Histomorphometric analysis of bone remodeling. In: Bilezikian JP, Raisz LG, Rodan GA, eds. Principles of bone biology. San Diego, Calif: Academic Press, 2002; 303–319.

22. Hernandez CJ, Beaupré GS, Carter DR. A model of mechanobiologic and metabolic influences on bone adaptation. J Rehabil Res Dev 2000;37(2):235–244.

23. Odvina CV, Zerwekh JE, Rao DS, Maalouf N, Gottschalk FA, Pak CY. Severely suppressed bone turnover: a potential complication of alendronate therapy. J Clin Endocrinol Metab 2005;90(3):1294–1301.

24. Goh SK, Yang KY, Koh JS, et al. Subtrochanteric insufficiency fractures in patients on alendronate therapy: a caution. J Bone Joint Surg Br 2007;89(3):349–353.

25. Benjamin M, Toumi H, Ralphs JR, Bydder G, Best TM, Milz S. Where tendons and ligaments meet bone: attachment sites ('entheses') in relation to exercise and/or mechanical load. J Anat 2006;208(4):471–490.

26. Davison KS, Siminoski K, Adachi JD, et al. Bone strength: the whole is greater than the sum of its parts. Semin Arthritis Rheum 2006;36(1):22–31.

27. Oxlund H, Mosekilde L, Ortoft G. Reduced concentration of collagen reducible cross links in human trabecular bone with respect to age and osteoporosis. Bone 1996;19(5):479–484.

28. Boivin G, Meunier PJ. The degree of mineralization of bone tissue measured by computerized quantitative contact microradiography. Calcif Tissue Int 2002;70(6):503–511.

29. Currey JD, Brear K, Zioupos P. The effects of ageing and changes in mineral content in degrading the toughness of human femora. J Biomech 1996;29(2):257–260.

30. Riggs BL, Hodgson SF, O'Fallon WM, et al. Effect of fluoride treatment on the fracture rate in postmenopausal women with osteoporosis. N Engl J Med 1990;322(12):802–809.

31. Freeman JJ, Wopenka B, Silva MJ, Pasteris JD. Raman spectroscopic detection of changes in bioapatite in mouse femora as a function of age and in vitro fluoride treatment. Calcif Tissue Int 2001;68(3):156–162.

32. Huber M, Trattnig S, Lintner F. Anatomy, biochemistry, and physiology of articular cartilage. Invest Radiol 2000;35(10):573–580.

33. Freeman PM, Natarajan RN, Kimura JH, Andriacchi TP. Chondrocyte cells respond mechanically to compressive loads. J Orthop Res 1994;12(3):311–320.

34. Glaser C, Putz R. Functional anatomy of articular cartilage under compressive loading: quantitative aspects of global, local and zonal reactions of the collagenous network with respect to the surface integrity. Osteoarthritis Cartilage 2002;10(2):83–99.

35. Weiss C, Rosenberg L, Helfet AJ. An ultrastructural study of normal young adult human articular cartilage. J Bone Joint Surg Am 1968;50(4):663–674.

36. Alms M. Fracture mechanics. J Bone Joint Surg Br 1961;43-B:162–166.

37. Nordin M, Frankel VH. Biomechanics of bone. In: Nordin M, Frankel VH, eds. Basic biomechanics of the musculoskeletal system. 2nd ed. Baltimore, Md: Lippincott Williams & Wilkins, 2001; 26–59.

38. Gitajn IL, Rodriguez EK. Biomechanics of musculoskeletal injury, biomechanics in applications. In: Klika V, ed. INTECH Web site. http://www.intechopen.com/books/biomechanics-in-applications/biomechanics-of-musculoskeletal-injury. Published 2011. Accessed September 27, 2014.

39. Dempster DW. Bone microarchitecture and strength. Osteoporos Int 2003;14(Suppl 5):S54–S56.

40. Shirazi R, Shirazi-Adl A, Hurtig M. Role of cartilage collagen fibrils networks in knee joint biomechanics under compression. J Biomech 2008;41(16):3340–3348.

41. Linn FC, Sokoloff L. Movement and composition of interstitial fluid of cartilage. Arthritis Rheum 1965;8:481–494.

42. Mow VC, Holmes MH, Lai WM. Fluid transport and mechanical properties of articular cartilage: a review. J Biomech 1984; 17(5):377–394.

43. Arøen A, Løken S, Heir S, et al. Articular cartilage lesions in 993 consecutive knee arthroscopies. Am J Sports Med 2004; 32(1):211–215.

44. Hjelle K, Solheim E, Strand T, Muri R, Brittberg M. Articular cartilage defects in 1,000 knee arthroscopies. Arthroscopy 2002;18(7):730–734.

45. Curl WW, Krome J, Gordon ES, Rushing J, Smith BP, Poehling GG. Cartilage injuries: a review of 31,516 knee arthroscopies. Arthroscopy 1997;13(4):456–460.

46. Mow VC, Zhu W, Ratcliffe A. Structure and function of articular cartilage and me-

niscus. In: Mow VC, Hayes WC, eds. Basic orthopaedic biomechanics. New York, NY: Raven, 1991; 143–198.

47. Farmer JM, Martin DF, Boles CA, Curl WW. Chondral and osteochondral injuries. Diagnosis and management. Clin Sports Med 2001;20(2):299–320.

48. Borrelli J Jr, Ricci WM. Acute effects of cartilage impact. Clin Orthop Relat Res 2004;(423):33–39.

49. Bae WC, Lewis CW, Levenston ME, Sah RL. Indentation testing of human articular cartilage: effects of probe tip geometry and indentation depth on intra-tissue strain. J Biomech 2006;39(6):1039–1047.

50. Mow VC, Kuei SC, Lai WM, Armstrong CG. Biphasic creep and stress relaxation of articular cartilage in compression? Theory and experiments. J Biomech Eng 1980; 102(1):73–84.

51. Frank EH, Grodzinsky AJ. Cartilage electromechanics. II. A continuum model of cartilage electrokinetics and correlation with experiments. J Biomech 1987;20(6): 629–639.

52. Ewers BJ, Jayaraman VM, Banglmaier RF, Haut RC. Rate of blunt impact loading affects changes in retropatellar cartilage and underlying bone in the rabbit patella. J Biomech 2002;35(6):747–755.

53. Gallo RA, Mosher TJ. Imaging of cartilage and osteochondral injuries: a case-based review. Clin Sports Med 2013;32(3):477–505.

54. Loening AM, James IE, Levenston ME, et al. Injurious mechanical compression of bovine articular cartilage induces chondrocyte apoptosis. Arch Biochem Biophys 2000; 381(2):205–212.

55. D'Lima DD, Hashimoto S, Chen PC, Colwell CW Jr, Lotz MK. Human chondrocyte apoptosis in response to mechanical injury. Osteoarthritis Cartilage 2001;9(8):712–719.

56. Kurz B, Jin M, Patwari P, Cheng DM, Lark MW, Grodzinsky AJ. Biosynthetic response and mechanical properties of articular cartilage after injurious compression. J Orthop Res 2001;19(6):1140–1146.

57. Clements KM, Bee ZC, Crossingham GV, Adams MA, Sharif M. How severe must repetitive loading be to kill chondrocytes in articular cartilage? Osteoarthritis Cartilage 2001;9(5):499–507.

58. Quinn TM, Allen RG, Schalet BJ, Perumbuli P, Hunziker EB. Matrix and cell injury due to sub-impact loading of adult bovine articular cartilage explants: effects of strain rate and peak stress. J Orthop Res 2001;19(2):242–249.

59. Patwari P, Gaschen V, James IE, et al. Ultrastructural quantification of cell death after injurious compression of bovine calf articular cartilage. Osteoarthritis Cartilage 2004;12(3):245–252.

60. Duda GN, Eilers M, Loh L, Hoffman JE, Kääb M, Schaser K. Chondrocyte death precedes structural damage in blunt impact trauma. Clin Orthop Relat Res 2001; (393):302–309.

61. Chen CT, Bhargava M, Lin PM, Torzilli PA. Time, stress, and location dependent chondrocyte death and collagen damage in cyclically loaded articular cartilage. J Orthop Res 2003;21(5):888–898.

62. Li X, Kuo D, Theologis A, et al. Cartilage in anterior cruciate ligament-reconstructed knees: MR imaging T1rho and T2--initial experience with 1-year follow-up. Radiology 2011;258(2):505–514.

63. Potter HG, Jain SK, Ma Y, Black BR, Fung S, Lyman S. Cartilage injury after acute, isolated anterior cruciate ligament tear: immediate and longitudinal effect with clinical/MRI follow-up. Am J Sports Med 2012;40(2):276–285.

64. Tiderius CJ, Olsson LE, Nyquist F, Dahlberg L. Cartilage glycosaminoglycan loss in the acute phase after an anterior cruciate ligament injury: delayed gadolinium-enhanced magnetic resonance imaging of cartilage and synovial fluid analysis. Arthritis Rheum 2005;52(1):120–127.

65. Tomatsu T, Imai N, Takeuchi N, Takahashi K, Kimura N. Experimentally produced fractures of articular cartilage and bone: the effects of shear forces on the pig knee. J Bone Joint Surg Br 1992;74(3):457–462.

66. Mosher TJ. MRI of osteochondral injuries of the knee and ankle in the athlete. Clin Sports Med 2006;25(4):843–866.

67. Outerbridge RE. The etiology of chondromalacia patellae. J Bone Joint Surg Br 1961;43-B:752–757.

68. Noyes FR, Bassett RW, Grood ES, Butler DL. Arthroscopy in acute traumatic hemarthrosis of the knee: incidence of anterior cruciate tears and other injuries. J Bone Joint Surg Am 1980;62(5):687–695, 757.

69. Cameron ML, Briggs KK, Steadman JR. Reproducibility and reliability of the outerbridge classification for grading chondral lesions of the knee arthroscopically. Am J Sports Med 2003;31(1):83–86.

70. Brittberg M. Evaluation of cartilage injuries and cartilage repair. Osteologie 2000;9: 17–25.

71. Brittberg M, Winalski CS. Evaluation of cartilage injuries and repair. J Bone Joint Surg Am 2003;85-A(Suppl 2):58–69.

72. Kijowski R, Blankenbaker DG, Davis KW, Shinki K, Kaplan LD, De Smet AA. Comparison of 1.5- and 3.0-T MR imaging for evaluating the articular cartilage of the knee joint. Radiology 2009;250(3):839–848.

73. Bredella MA, Tirman PF, Peterfy CG, et al. Accuracy of T2-weighted fast spin-echo MR imaging with fat saturation in detecting cartilage defects in the knee: comparison with arthroscopy in 130 patients. AJR Am J Roentgenol 1999;172(4):1073–1080.

74. Peterfy CG, Guermazi A, Zaim S, et al. Whole-Organ Magnetic Resonance Imaging Score (WORMS) of the knee in osteoarthritis. Osteoarthritis Cartilage 2004;12(3):177–190.

75. Potter HG, Koff MF. MR Imaging tools to assess cartilage and joint structures. HSS J 2012;8(1):29–32.

76. Gold GE, Burstein D, Dardzinski B, Lang P, Boada F, Mosher T. MRI of articular cartilage in OA: novel pulse sequences and compositional/functional markers. Osteoarthritis Cartilage 2006;14(Suppl A):A76–A86.

77. Williams A, Gillis A, McKenzie C, et al. Glycosaminoglycan distribution in cartilage as determined by delayed gadolinium-enhanced MRI of cartilage (dGEMRIC): potential clinical applications. AJR Am J Roentgenol 2004;182(1):167–172.

78. Wheaton AJ, Dodge GR, Borthakur A, Kneeland JB, Schumacher HR, Reddy R. Detection of changes in articular cartilage proteoglycan by T(1rho) magnetic resonance imaging. J Orthop Res 2005;23(1):102–108.

79. Xia Y, Moody JB, Burton-Wurster N, Lust G. Quantitative in situ correlation between microscopic MRI and polarized light microscopy studies of articular cartilage. Osteoarthritis Cartilage 2001;9(5):393–406.

80. Madry H, van Dijk CN, Mueller-Gerbl M. The basic science of the subchondral bone. Knee Surg Sports Traumatol Arthrosc 2010;18(4):419–433.

81. Radin EL, Rose RM. Role of subchondral bone in the initiation and progression of cartilage damage. Clin Orthop Relat Res 1986;(213):34–40.

82. Hert J. A new attempt at the interpretation of the functional architecture of the cancellous bone. J Biomech 1994;27(2):239–242.

83. Barak MM, Lieberman DE, Hublin JJ. A Wolff in sheep's clothing: trabecular bone adaptation in response to changes in joint loading orientation. Bone 2011;49(6):1141–1151.

84. Lanyon LE. Analysis of surface bone strain in the calcaneus of sheep during normal locomotion: strain analysis of the calcaneus. J Biomech 1973;6(1):41–49.

85. Lanyon LE. Experimental support for the trajectorial theory of bone structure. J Bone Joint Surg Br 1974;56(1):160–166.

86. Bouvier M. Application of in vivo bone strain measurement techniques to problems of skeletal adaptations. Am J Phys Anthropol 1985;28(Suppl 6):237–248.

87. Su SC, Skedros JG, Bachus KN, Bloebaum RD. Loading conditions and cortical bone construction of an artiodactyl calcaneus. J Exp Biol 1999;202(Pt 22):3239–3254.

88. Skedros JG, Baucom SL. Mathematical analysis of trabecular 'trajectories' in apparent trajectorial structures: the unfortunate historical emphasis on the human proximal femur. J Theor Biol 2007;244(1):15–45.

89. Beck TJ, Ruff CB, Warden KE, Scott WW Jr, Rao GU. Predicting femoral neck strength from bone mineral data: a structural approach. Invest Radiol 1990;25(1):6–18.

90. Cristofolini L, Viceconti M, Cappello A, Toni A. Mechanical validation of whole bone composite femur models. J Biomech 1996;29(4):525–535.

91. Pramudito JT, Soegijoko S, Mengko TR, Muchtadi FI, Wachjudi RG. Trabecular pattern analysis of proximal femur radiographs for osteoporosis detection. J Biomed Pharm Eng 2007;1(1):45–51.

92. Jang IG, Kim IY. Computational study of Wolff's law with trabecular architecture in the human proximal femur using topology optimization. J Biomech 2008;41(11):2353–2361.

93. Carter DR, Orr TE, Fyhrie DP. Relationships between loading history and femoral cancellous bone architecture. J Biomech 1989;22(3):231–244.

94. Deutsch AL, Mink JH, Shellock FG. Magnetic resonance imaging of injuries to bone and articular cartilage: emphasis on radiographically occult abnormalities. Orthop Rev 1990;19(1):66–75.

95. Murphy BJ, Smith RL, Uribe JW, Janecki CJ, Hechtman KS, Mangasarian RA. Bone signal abnormalities in the posterolateral tibia and lateral femoral condyle in complete tears of the anterior cruciate ligament: a specific sign? Radiology 1992;182(1):221–224.

96. Cox LG, Lagemaat MW, van Donkelaar CC, et al. The role of pressurized fluid in subchondral bone cyst growth. Bone 2011;49(4):762–768.

97. Rangger C, Kathrein A, Freund MC, Klestil T, Kreczy A. Bone bruise of the knee: histology and cryosections in 5 cases. Acta Orthop Scand 1998;69(3):291–294.

98. Wong A, Grando H, Fliszar E, Pathria M, Chang EY, Resnick D. Intramedullary fat globules related to bone trauma: a new MR imaging finding. Skeletal Radiol 2014;43(12):1713–1719.

99. Watson AJ. Genesis of fat emboli. J Clin Pathol Suppl (R Coll Pathol) 1970;4:132–142.

100. Gupta HS, Zioupos P. Fracture of bone tissue: the 'hows' and the 'whys'. Med Eng Phys 2008;30(10):1209–1226.

101. Doblaré M, García JM, Gómez MJ. Modelling (sic) bone tissue fracture and healing: a review. Eng Fract Mech 2004;71(13-14):1809–1840.

102. Bae WC, Chen PC, Chung CB, Masuda K, D'Lima D, Du J. Quantitative ultrashort echo time (UTE) MRI of human cortical bone: correlation with porosity and biomechanical properties. J Bone Miner Res 2012;27(4):848–857.

103. Burr DB, Schaffler MB, Frederickson RG. Composition of the cement line and its possible mechanical role as a local interface in human compact bone. J Biomech 1988;21(11):939–945.

104. Skedros JG, Holmes JL, Vajda EG, Bloebaum RD. Cement lines of secondary osteons in human bone are not mineral-deficient: new data in a historical perspective. Anat Rec A Discov Mol Cell Evol Biol 2005;286(1):781–803.

105. Steiniche T, Hauge EM. Normal structure and function of bone. In: An YH, Martin KL, eds. Handbook of histology methods for bone and cartilage. Totowa, NJ: Humana, 2003; 59–72.

106. Ritchie RO, Kinney JH, Kruzic JJ, Nalla RK. A fracture mechanics and mechanistic approach to the failure of cortical bone. Fatigue Fract Engng Mater Struct 2005;28(4):345–371.

107. Ritchie RO, Buehler MJ, Hansma P. Plasticity and toughness in bone. Phys Today 2009;62(6):41–46.

108. Launey ME, Buehler MJ, Ritchie RO. On the mechanistic origins of toughness in bone. Annu Rev Mater Res 2010;40:25–53.

109. Koester KJ, Ager JW 3rd, Ritchie RO. The true toughness of human cortical bone measured with realistically short cracks. Nat Mater 2008;7(8):672–677.

110. Fratzl P. Bone fracture: when the cracks begin to show. Nat Mater 2008;7(8):610–612.

111. Pegrum J, Crisp T, Padhiar N. Diagnosis and management of bone stress injuries of the lower limb in athletes. BMJ 2012;344(7854):e2511.

112. Seeman E, Delmas PD. Bone quality: the material and structural basis of bone strength and fragility. N Engl J Med 2006;354(21):2250–2261.

113. Umans HR, Kaye JJ. Longitudinal stress fractures of the tibia: diagnosis by magnetic resonance imaging. Skeletal Radiol 1996;25(4):319–324.

114. Williams M, Laredo JD, Setbon S, et al. Unusual longitudinal stress fractures of the femoral diaphysis: report of five cases. Skeletal Radiol 1999;28(2):81–85.

115. Craig JG, Widman D, van Holsbeeck M. Longitudinal stress fracture: patterns of edema and the importance of the nutrient foramen. Skeletal Radiol 2003;32(1):22–27.

116. Pathria MN. Radiologic analysis of trauma. In: Naham A, Melvin JW, eds. Accidental injury: biomechanics and prevention. 2nd ed. New York, NY: Springer-Verlag, 2001; 103–120.

117. Rogers LF. Skeletal biomechanics. In: Rogers LF, ed. Radiology of skeletal trauma. New York, NY: Churchill Livingstone, 1992; 19–28.

118. Anderson MW, Greenspan A. Stress fractures. Radiology 1996;199(1):1–12.

119. Beck BR, Bergman AG, Miner M, et al. Tibial stress injury: relationship of radiographic, nuclear medicine bone scanning, MR imaging, and CT severity grades to clinical severity and time to healing. Radiology 2012;263(3):811–818.

120. Pepper M, Akuthota V, McCarty EC. The pathophysiology of stress fractures. Clin Sports Med 2006;25(1):1–16, vii.

121. Burghardt AJ, Link TM, Majumdar S. High-resolution computed tomography for clinical imaging of bone microarchitecture. Clin Orthop Relat Res 2011;469(8):2179–2193.

122. Yamamoto T, Bullough PG. Spontaneous osteonecrosis of the knee: the result of subchondral insufficiency fracture. J Bone Joint Surg Am 2000;82(6):858–866.

123. Popp KL, Hughes JM, Smock AJ, et al. Bone geometry, strength, and muscle size in runners with a history of stress fracture. Med Sci Sports Exerc 2009;41(12):2145–2150.